ON THE SECOND-ORDER STATISTICS OF THE INSTANTANEOUS MUTUAL INFORMATION OF TIME-VARYING FADING CHANNELS

Shuangquan Wang, Ali Abdi

New Jersey Institute of Technology
Department of Electrical and Computer Engineering
University Heights, Newark, NJ 07102
Email: {sw27, ali.abdi}@njit.edu

ABSTRACT

In this paper, the instantaneous mutual information random process is defined and its second-order statistics such as the autocorrelation and autocovariance functions, level crossing rate, and average outage duration are studied in Rayleigh fading channels with non-isotropic scattering. Closed-form expressions and simple approximate results are derived for the statistics of the instantaneous mutual information random process, and their accuracies are verified via Monte Carlo simulations.

1. INTRODUCTION

The increasing demand for wireless communication over time-varying channels has motivated further investigation of the channel dynamics and its statistical behavior. There are numerous studies on the temporal second-order characteristics of a variety of terrestrial [1]–[6] and satellite channels [7], such as correlation function, level crossing rate (LCR), and average fade duration. However, the dynamics of the *instantaneous mutual information* (IMI) of a time-varying fading channel has not been studied so far, to the best of our knowledge. For example, the outage probability of a fading channel gives the probability of the IMI to be smaller than a threshold [8]. Nevertheless, it does not show how long the IMI stays below the threshold. This is in fact the average outage duration (AOD) of IMI of a time-varying channel, different from the outage probability. In this paper we define and calculate important second-order statistics of the IMI, which give us a more detailed picture of time-varying channels, required for the design of proper signaling schemes.

The rest of the paper is organized as follows. Sec. 2 introduces the channel model and defines the instantaneous mutual information random process, whereas the distributions of scatterers and angle-of-arrival (AoA) are discussed in Sec. 3. Sec. 4 is devoted to the autocorrelation function (ACF) and autocovariance function (AVF) of the IMI. The LCR and AOD of the IMI are derived in Sec. 5 and 6, respectively. Numerical results are presented in Sec. 7, which verify the accuracy of the theoretical results. Finally, the concluding remarks are given in Sec. 8.

2. THE CHANNEL MODEL AND IMI

In a flat Rayleigh fading channel, the lowpass complex envelope of the channel response $h(t)$ is a zero-mean complex Gaussian random process, which can be represented as

$$h(t) = \alpha(t)\exp[-j\Phi(t)], \tag{1}$$

where $\alpha(t)$ and $\Phi(t)$ are real random processes, and $j = \sqrt{-1}$. At any time t, $\alpha(t)$ has Rayleigh distribution and $\Phi(t)$ is distributed uniformly over $[0, 2\pi)$. Without loss of generality, we assume the Rayleigh channel has unit power, i.e., $\mathbb{E}[\alpha^2(t)] = 1$, where $\alpha(t)$ is the envelope of $h(t)$, and $\mathbb{E}(\cdot)$ is the mathematical expectation.

If the additive noise is Gaussian, and if the perfect channel state information $h(t)$ is available at the receiver only, the ergodic channel capacity is defined as [8]–[11]

$$\overline{C} = \mathbb{E}\{\log_2[1 + \eta\alpha^2(t)]\} \tag{2}$$

bits/s/Hz, where η is the signal-to-noise ratio (SNR).

In the above equation, at any given time t, $\log_2[1 + \eta\alpha^2(t)]$ is a random variable as it depends on the fading amplitude $\alpha(t)$ [8]. We define the IMI random process as

$$C(t) = \log_2[1 + \eta\alpha^2(t)]. \tag{3}$$

We will study its second-order statistics such as autocorrelation, autocovariance, LCR and AOD in the following sections.

3. THE ANGLE OF ARRIVAL DISTRIBUTION

To model the distribution of the angle-of-arrival of waves impinging on either the base station (BS) or mobile station

(MS), we use multiple von Mises distributions. The von Mises probability density function (PDF) has proven to be a flexible model for the AoA at both BS [12] and MS [6]. For example, in the macrocellular environment shown in Fig. 1, one von Mises distribution is enough for the BS AoA, whereas two von Mises distributions are needed to model the two clusters of scatterers around the MS. In general, we write the probability density function of the AoA in the azimuth plane as the superposition of N von Mises PDFs

$$p(\theta) = \sum_{n=1}^{N} P_n \frac{\exp[\kappa_n \cos(\theta - \theta_n)]}{2\pi I_0(\kappa_n)}, \quad \theta \in [0, 2\pi), \quad (4)$$

where $I_k(z) = \frac{1}{\pi}\int_0^{\pi} e^{z\cos\theta}\cos(k\theta)\mathrm{d}\theta$ is the k^{th} order modified Bessel function of the first kind. θ_n is the mean AoA of the n^{th} cluster, κ_n controls the width of the n^{th} cluster, and P_n represents the contribution of the n^{th} cluster, such that $\sum_{n=1}^{N} P_n = 1, 0 < P_n \leqslant 1$. If $\kappa_n = 0, \forall n$, (4) simplifies to $p(\theta) = \frac{1}{2\pi}, \theta \in [0, 2\pi)$, which is the Clarke's 2-D isotropic scattering model. The AoA PDF given in (4) is generally enough to model any measured AoA. Furthermore, it provides closed-form and mathematically-tractable expressions for the channel correlation functions [6][12].

4. ACF AND AVF OF THE IMI

In this section, first we concentrate on the ACF of the IMI, given in (3). The ACF is defined by

$$\begin{aligned} r_C(\tau) &= \mathbb{E}[C(t)C(t-\tau)] \\ &= (\log_2 e)^2 \mathbb{E}[\ln(1+\eta x_1)\ln(1+\eta x_2)], \end{aligned} \quad (5)$$

where $\ln(\cdot)$ is the natural logarithm with $x_1 = \alpha^2(t)$ and $x_2 = \alpha^2(t-\tau)$, x_1 and x_2 have a joint Chi-square PDF with 2 degrees of freedom, given by [13, pp. 21, (3.17)]

$$p(x_1, x_2) = \frac{\lambda_\tau}{2} e^{-\lambda_\tau(x_1+x_2)} I_0(2\lambda_\tau \varrho_\tau \sqrt{x_1 x_2}), \quad (6)$$

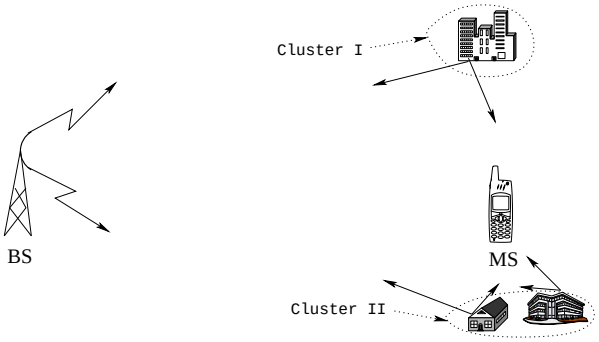

Fig. 1. The scattering environment around the MS

where $\lambda_\tau = \frac{1}{2(1-\varrho_\tau^2)}$, $\varrho_\tau = |\rho_h(\tau)|$, and the channel correlation coefficient $\rho_h(\tau)$ and spectrum of Rayleigh fading are given by

$$\begin{aligned} \rho_h(\tau) &= E[h(t)h^*(t-\tau)], \\ &= \sum_{n=1}^{N} P_n \frac{I_0(\sqrt{\kappa_n^2 - 4\pi^2 f_m^2 \tau^2 + j4\pi\kappa_n f_m \tau \cos\theta_n})}{I_0(\kappa_n)}, \end{aligned} \quad (7)$$

and

$$\begin{aligned} S_h(f) = &\sum_{n=1}^{N} P_n \frac{\exp(\kappa_n f \cos\theta_n / f_m)}{\pi\sqrt{f_m^2 - f^2} I_0(\kappa_n)} \\ &\times \cosh[\kappa_n \sqrt{1-(f/f_m)^2}\sin\theta_n], |f| \leqslant f_m, \end{aligned} \quad (8)$$

respectively, in which f_m is the maximum Doppler frequency, and $\cosh(z) = \frac{1}{2}(e^z + e^{-z})$ is the hyperbolic cosine function. Equations (7) and (8) are derived by extending some formulas in [6], according to (4). If $\kappa_n = 0, \forall n$, (7) and (8) can be simplified to $\rho_h(\tau) = I_0(j2\pi f_m \tau) = J_0(2\pi f_m \tau)$ and $S_h(f) = \frac{1}{2\pi\sqrt{f_m^2 - f^2}}, |f| \leqslant f_m$, respectively, which correspond to the classic Clarke's model. Also, (8) will be used to generate the Rayleigh flat fading channel with non-isotropic scattering for Monte Carlo simulations in Sec. 7.

In general, it seems hard to calculate (5) for an arbitrary SNR. So, in this paper, we consider the low and high SNR regimes. Based on the properties of (6), one can simplify (5) to

$$\frac{r_C(\tau)}{(\log_2 e)^2} \approx \begin{cases} \mathbb{E}(\eta^2 x_1 x_2) & \eta \ll 1, \\ \mathbb{E}[\ln(\eta x_1)\ln(\eta x_2)] & \eta \gg 1. \end{cases} \quad (9)$$

In the following two subsections, we use (9) to derive closed-form expressions for $r_C(\tau)$ in both low- and high-SNR regimes, by using the series representation of $I_0(t)$ [14, 8.447.1]

$$I_0(t) = \sum_{n=0}^{\infty} \frac{t^{2n}}{(n!)^2 2^{2n}}, \quad (10)$$

4.1. Low SNR

If $\eta \ll 1$, based on (6), (9) and (10), we have

$$\frac{r_C(\tau)}{(\log_2 e)^2} \approx \frac{\lambda_\tau}{2} \sum_{n=0}^{\infty} \frac{\Xi_1^2(n, \eta, \lambda_\tau)}{(\lambda_\tau \varrho_\tau)^{-2n}(n!)^2}, \quad (11)$$

where $\Xi_1(n, \eta, \lambda_\tau)$ is defined as $\eta\int_0^{\infty} x^{n+1} e^{-\lambda_\tau x}\mathrm{d}x$, which can be simplified to

$$\Xi_1(n, \eta, \lambda_\tau) = \eta \frac{(n+1)!}{\lambda_\tau^{n+2}}. \quad (12)$$

By replacing $\Xi_1(n,\eta,\lambda_\tau)$ in (11) with (12), we obtain

$$\begin{aligned}\frac{r_C(\tau)}{(\log_2 e)^2} &\approx \frac{\lambda_\tau}{2}\sum_{n=0}^{\infty}\frac{(\lambda_\tau\varrho_\tau)^{2n}}{(n!)^2}\left[\eta\frac{(n+1)!}{\lambda_\tau^{n+2}}\right]^2 \\ &= \frac{\eta^2}{2\lambda_\tau^3\varrho_\tau^2}\sum_{n=1}^{\infty}n^2\varrho_\tau^{2n}.\end{aligned} \tag{13}$$

Using 0.114 [14, pp. 1] and $\lim_{n\to\infty} n^k\varrho_\tau^{2n}=0$, where k is an integer and $\varrho_\tau<1$, finally the ACF, normalized such that $r_C(0)=1$, can be written as

$$r_C(\tau)\approx\frac{1}{2}\left(1+\varrho_\tau^2\right). \tag{14}$$

Moreover, the AVF defined by $\rho_C(\tau)=r_C(\tau)-\overline{C}^2$, normalized such that $\rho_C(0)=1$, is given by

$$\rho_C(\tau)\approx\varrho_\tau^2. \tag{15}$$

With isotropic scattering, $N=1$ and $\kappa_1=0$, (15) simplifies to $J_0^2(2\pi f_m\tau)$, where $J_0(\cdot)$ is the zero-order Bessel function of the first kind.

4.2. High SNR

If $\eta\gg 1$, based on (6), (9) and (10), we obtain

$$\frac{r_C(\tau)}{(\log_2 e)^2}\approx\frac{\lambda_\tau}{2}\sum_{n=0}^{\infty}\frac{\Xi_2^2(n,\eta,\lambda_\tau)}{(\lambda_\tau\varrho_\tau)^{-2n}(n!)^2}, \tag{16}$$

where $\Xi_2(n,\eta,\lambda_\tau)$ is defined as $\int_0^\infty x^n(\ln\eta+\ln x)e^{-\lambda_\tau x}\mathrm{d}x$. Using 4.352.2 [14, pp. 604], we obtain

$$\begin{aligned}\Xi_2(n,\eta,\lambda_\tau) &\approx \int_0^\infty x^n(\ln\eta+\ln x)e^{-\lambda_\tau x}\mathrm{d}x, \\ &= \frac{n!}{\lambda_\tau^{n+1}}\left(\ln\frac{\eta}{\lambda_\tau\xi}+\sigma_n\right),\end{aligned} \tag{17}$$

where $\xi=e^\gamma$, $\gamma=0.577215\cdots$ is the Euler's constant [pp. xxx] [14], $\sigma_n=\sum_{k=1}^n\frac{1}{k}$ for $n\geqslant 1$, and $\sigma_0=0$. After lengthy algebraic calculations, finally the normalized ACF in the high-SNR regime is shown to be

$$\begin{aligned}r_C(\tau) &\approx 1-\frac{6\int_1^{\varrho_\tau^2}\frac{\ln(1-t)}{t}\mathrm{d}t}{\pi^2+6\ln^2\left(\frac{2\eta}{\xi}\right)}, \\ &= \frac{\mathrm{dilog}(1-\varrho_\tau^2)+\ln^2\left(\frac{2\eta}{\xi}\right)}{\frac{\pi^2}{6}+\ln^2\left(\frac{2\eta}{\xi}\right)},\end{aligned} \tag{18}$$

where $\mathrm{dilog}(x)=\int_1^x\frac{\ln t}{1-t}\mathrm{d}t$.

The normalized AVF can be written as

$$\rho_C(\tau)\approx\frac{6\,\mathrm{dilog}(1-\varrho_\tau^2)}{\pi^2}. \tag{19}$$

With isotropic scattering, (19) reduces to

$$\rho_C(\tau)=\frac{6\,\mathrm{dilog}[1-J_0^2(2\pi f_m\tau)]}{\pi^2}. \tag{20}$$

5. LCR OF THE IMI

By noting the fact that $C(t)$ in (3) is a nonlinear transformation of $\alpha(t)$, and based on the LCR of $\alpha(t)$ [4], we have shown that the LCR of $C(t)$, with respect to the threshold C_{th}, is given by

$$\begin{aligned}N(C_{th}) &= 2\sqrt{\pi(2^{C_{th}}-1)/\eta}\exp\left(-\frac{2^{C_{th}}-1}{\eta}\right)f_m \\ &\times\left\{\sum_{n=1}^{N}\frac{2\sin^2\theta_n I_1(\kappa_n)+\kappa_n\cos^2\theta_n[I_0(\kappa_n)+I_2(\kappa_n)]}{2\kappa_n I_0(\kappa_n)/P_n}\right. \\ &\left.-\left[\sum_{n=1}^{N}\frac{P_n\cos\theta_n I_1(\kappa_n)}{I_0(\kappa_n)}\right]^2\right\}^{\frac{1}{2}},\end{aligned} \tag{21}$$

In the case of isotropic scattering, and according to the identity $\lim_{\kappa\to 0}\frac{I_1(\kappa)}{\kappa I_0(\kappa)}=\frac{1}{2}$, the IMI LCR (21) reduces to

$$N(C_{th})=f_m\sqrt{2\pi(2^{C_{th}}-1)/\eta}\exp\left(-\frac{2^{C_{th}}-1}{\eta}\right). \tag{22}$$

6. AOD OF THE IMI

Based on the relationship between C and α in (3), the cumulative distribution function (CDF) of C is shown to be

$$F(C)=1-\exp\left[(2^C-1)/\eta\right]. \tag{23}$$

The AOD of the IMI is therefore given by[1]

$$\bar{t}(C_{th})=F(C_{th})/N(C_{th}), \tag{24}$$

where $N(\cdot)$ and $F(\cdot)$ are given by (21) and (23), respectively. With the isotropic scattering, the AOD, normalized by f_m, is

$$\bar{t}(C_{th})f_m=\frac{\sqrt{\eta}\left[\exp\left(\frac{2^{C_{th}}-1}{\eta}\right)-1\right]}{\sqrt{2\pi(2^{C_{th}}-1)}}. \tag{25}$$

7. NUMERICAL RESULTS

In this paper, we have used the spectral method of [15] to simulate the Rayleigh flat fading channel with non-isotropic scattering. For all simulations, the maximum Doppler frequency shift f_m is set to 1Hz[2].

For ACF and AVF simulation at the MS, we set $\eta=-30$dB for low SNR and $\eta=30$dB for high SNR. For isotropic scattering simulation in Fig. 2, we set $\kappa_1=0$

[1]The concept is similar to the average envelope fade duration, whose formula is given by (2.106) [3, pp. 66]

[2]The specific value of f_m is not critical in this study, since it appears as a scaling factor, such as $2\pi f_m\tau$ in all the correlation and covariance expressions, as well as LCR and AOD in (21) and (24), respectively.

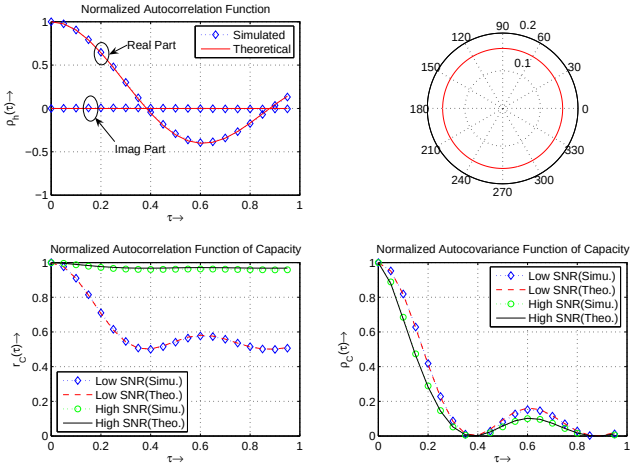

Fig. 2. ACF and AVF of the channel $h(t)$ and the IMI $C(t)$, with isotropic scattering.

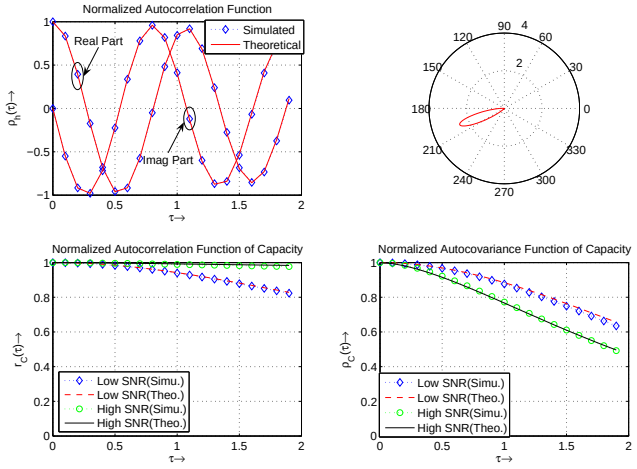

Fig. 4. ACF and AVF of the channel $h(t)$ and the IMI $C(t)$, with highly non-isotropic scattering.

and $P_1 = 1$, whereas for non-isotropic scattering simulation in Fig. 3, we consider two clusters around the MS, such that $[\kappa_1, \kappa_2] = [5, 20]$, $[\theta_1, \theta_2] = \frac{\pi}{180}[50, 200]$ and $[P_1, P_2] = [0.7, 0.3]$. The upper left figure shows the real and imaginary parts of $\rho_h(\tau)$, given by (7), the upper right figure is polar plot of the AoA PDF $p(\theta)$ in (4), the lower left figure is the ACF of $C(t)$ at both low and high SNRs, and finally, the lower right shows the AVF.

Interestingly, in both propagation scenarios, low and high SNR, AVFs of the IMI are very close. To see the effect of a highly directional reception, Fig. 4 is generated with one cluster, $N = 1$, such that $\kappa = 40$ and $\theta = \frac{10\pi}{9}$. Clearly the values of AVFs of the IMI are significantly increased, when compared with Fig. 2 and 3. Based on Fig. 2-4, we can conclude that the approximations given in subsections 4.1 and 4.2 are accurate in the low- and high-SNR regimes, respectively.

For LCR and AOD, we set the SNR η to 0dB. The isotropic scattering scenario is shown in Fig. 5, whereas for the non-isotropic scattering scenario in Fig. 6, three clusters around the MS are considered such that $[\kappa_1, \kappa_2, \kappa_3] = [2, 20, 3]$, $[\theta_1, \theta_2, \theta_3] = \frac{\pi}{180}[10, 110, 265]$ and $[P_1, P_2, P_3] = [0.45, 0.2, 0.35]$.

In Fig. 5-6, real and imaginary parts of $\rho_h(\tau)$ are shown in the upper left corner, the AoA is in the upper right corner, the LCR of the IMI given in (21) is plotted in the lower left corner, and finally the AOD of the IMI, presented in (24), is in the lower right corner.

By comparing Fig. 5 and 6, one can see larger values for LCR in the isotropic scattering scenario, which means more fluctuations of the IMI. On the other hand, the AOD of the

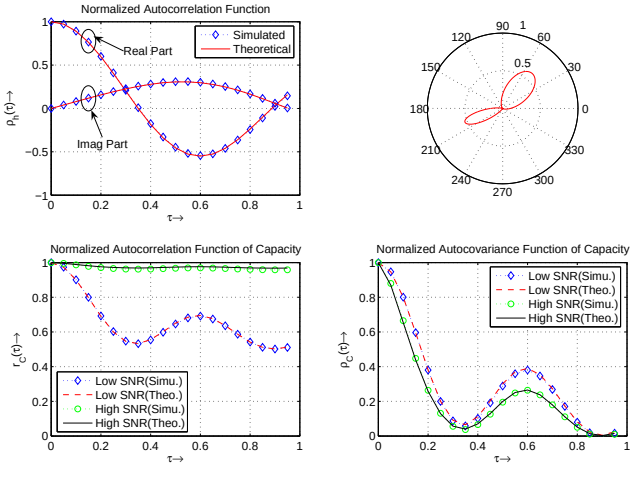

Fig. 3. ACF and AVF of the channel $h(t)$ and the IMI $C(t)$, with non-isotropic scattering.

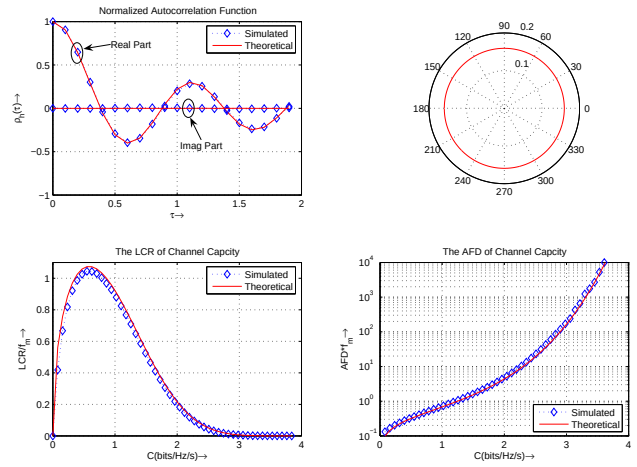

Fig. 5. LCR and AOD of the IMI, with isotropic scattering.

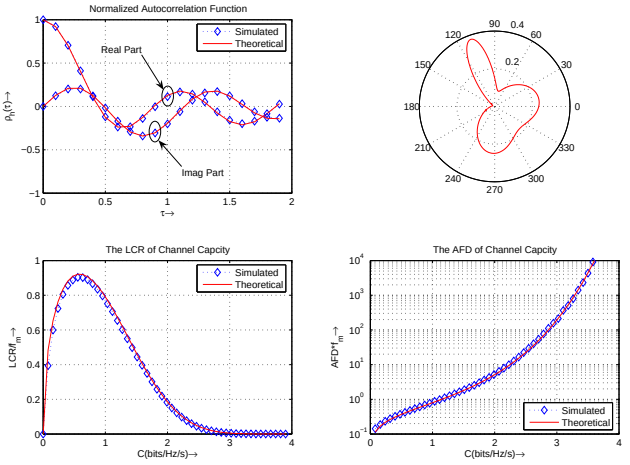

Fig. 6. LCR and AOD of the IMI, with non-isotropic scattering.

IMI does not appear to be very sensitive to the differences among the propagation examples considered.

8. CONCLUSION

In this paper, closed-form expressions for the level crossing rate and average outage duration of the IMI of a time-varying Rayleigh fading channel are derived, as well as correlation functions of the IMI at low and high SNR regimes. The analytical expressions, supported by Monte Carlo simulations, provide useful qualitative and quantitative information regarding the fluctuation of the IMI . For example, as the spread of the angle-of-arrival increases, IMI crossing rate increases according to our results, which means more fluctuations in the IMI. Furthermore, IMI values become less correlated. Quantification of the average outage duration of the IMI is another noteworthy outcome of this paper. For example, with isotropic scattering, the IMI remains below 3 bits/s/Hz for almost $100/f_m$ s, on average. At 900 MHz and for a car moving with 20 miles/h, this translates into a duration of 5 s.

9. REFERENCES

[1] S. O. Rice, "Mathematical analysis of random noise," *Bell Sys. Tech. J.*, vol. 24, pp. 46–156, 1945.

[2] W. C. Jakes and D. C. Cox, Eds., *Microwave Mobile Communications*. New York: IEEE Press, 1994.

[3] G. L. Stüber, *Principles of Mobile Communications (2nd ed.)*. Boston: Kluwer, 2000.

[4] A. Abdi, K. Wills, H. A. Barger, M. S. Alouini, and M. Kaveh, "Comparison of the level crossing rate and average fade duration of Rayleigh, Rice, and Nakagami fading models with mobile channel data," in *Proc. IEEE Veh. Technol. Conf.*, Boston, MA, 2000, pp. 1850–1857.

[5] N. Youssef, T. Munakata, and M. Takeda, "Fade statistics in Nakagami fading environments," in *Proc. IEEE Int. Symp. on Spread Spec. Tech. and App.*, Mainz, Germany, 1996, pp. 1244–1247.

[6] A. Abdi, J. A. Barger, and M. Kaveh, "A parametric model for the distribution of the angle of arrival and the associated correlation function and power spectrum at the mobile station," *IEEE Trans. Veh. Technol.*, vol. 51, pp. 425–434, 2002.

[7] A. Abdi, W. C. Lau, M. S. Alouini, and M. Kaveh, "A new simple model for land mobile satellite channels: First- and second-order statistics," *IEEE Trans. Wireless Commun.*, vol. 2, pp. 519–528, 2003.

[8] L. H. Ozarow, S. Shamai, and A. D. Wyner, "Information theoretic considerations for cellular mobile radio," *IEEE Trans. Veh. Technol.*, vol. 43, pp. 359–378, 1994.

[9] W. C. Y. Lee, "Estimate of channel capacity in Rayleigh fading environment," *IEEE Trans. Veh. Technol.*, vol. 39, pp. 187–189, 1990.

[10] C. Gunther, "Comment on "estimate of channel capacity in rayleigh fading environment"," *IEEE Trans. Veh. Technol.*, vol. 45, pp. 401–403, 1996.

[11] E. Biglieri, J. Proakis, and S. Shamai, "Fading channels: information-theoretic and communications aspects," *IEEE Trans. Inform. Theory*, vol. 44, pp. 2619–2692, 1998.

[12] A. Abdi and M. Kaveh, "A versatile spatio-temporal correlation function for mobile fading channels with non-isotropic scattering," in *Proc. IEEE Workshop Statistical Signal Array Processing*, Pocono Manor, PA, 2000, pp. 58–62.

[13] M. K. Simon, *Probability Distributions Involving Gaussian Random Variables: A Handbook for Engineers and Scientists*. Boston: Kluwer, 2002.

[14] I. S. Gradshteyn, I. M. Ryzhik, and A. Jeffrey, Eds., *Table of Integrals, Series, and Products (5th ed.)*. San Diego, CA: Academic, 1994.

[15] K. Acolatse and A. Abdi, "Efficient simulation of space-time correlated MIMO mobile fading channels," in *Proc. IEEE Veh. Technol. Conf.*, Orlando, FL, 2003, pp. 652–656.